ELSEVIER

Catalysis Today 78 (2003) 269–280

CATALYSIS TODAY

www.elsevier.com/locate/cattod

Vanadyl–aluminum binary phosphate: Al/V ratio influence on their structure and catalytic behavior in the 2-propanol conversion

F.M. Bautista*, J.M. Campelo, A. García, D. Luna, J.M. Marinas, A.A. Romero, M.T. Siles

Departamento Química Orgánica, Universidad de Córdoba, Campus de Rabanales, Edificio Marie Curie (C-3), E-14014 Córdoba, Spain

Abstract

The synthesis of aluminum–vanadium–phosphorus (AlVPO) systems by sol–gel method was carried out with several P/Al/V molar ratios. They were calcined at 450–550 °C as previously applied in the synthesis of amorphous $AlPO_4$ catalysts. Materials were characterized by chemical analysis, thermogravimetric analysis, X-ray diffraction, UV-Vis, ^{31}P and ^{27}Al MAS NMR, scanning electron microscopy and nitrogen adsorption. The textural properties and morphology of AlVPO materials were influenced by the Al/V ratio and thermal treatment. As the porosity of the solids decreased, both the BET surface areas as well as their primarily amorphous character did as well, while the vanadium content and calcination temperature increased. After calcination, the presence of two pure phosphate phases, $AlPO_4$ (α-cristobalite) and β-$VOPO_4$, was observed. Their catalytic behavior in the conversion of 2-propanol was studied. Both the activity for 2-propanol conversion and the selectivity values to propene and propanone were also greatly affected by the Al/V ratio values. Thus, the activity of the AlVPO systems increased with the aluminum content, whereas the 2-propanone selectivity decreased slightly. On the basis of kinetic study we conclude that dehydration to propene and dehydrogenation to propanone could proceed via different active sites and mechanisms.

Keywords: Vanadyl–aluminum binary phosphate; Catalyst preparation procedure; Catalyst characterization (XRD/UV-Vis/^{31}P, ^{27}Al MAS NMR/SEM); 2-Propanol conversion

1. Introduction

Vanadium is a key element in the formulation of catalysts utilized in the selective oxidation of hydrocarbons in the vapor phase. Among these catalysts, vanadium–phosphorus mixed oxides (V–P–O) have been the subject of extensive research, due principally to their widespread use as catalysts for the oxidation of *n*-butane to maleic anhydride (e.g. [1]). Several phases have been identified in different oxidation states of vanadium, depending on the formation of a specific phase mainly in the preparation method [2,3]. Furthermore, a wide variety of metal cations have been used as promoters not only of vanadyl pyrophosphate, which is considered to be critical for active and selective industrial catalysts, but also in other vanadyl phosphate phases [1,4,5].

On the other hand, aluminum phosphates, $AlPO_4$, have also been intensively studied as catalysts and metal supports in a great variety of gas or liquid-phase chemical processes. Furthermore, their texture, structure, and acid–base character as well as their catalytic properties can also be improved or modified by the incorporation of other metal oxides, e.g. TiO_2, Al_2O_3, V_2O_5, ZrO_2, B_2O_3 [6–10] and transition metal phosphates [11,12]. However, only a limited number of articles can be found in the literature concerning the

* Corresponding author. Fax: +34-957212066.
E-mail address: qo1baruf@uco.es (F.M. Bautista).

0920-5861/02/$ – see front matter © 2002 Elsevier Science B.V. All rights reserved.
PII: S0920-5861(02)00352-8

use of aluminum phosphate as the support for V–P–O catalysts, although it has been demonstrated to provide a good support material for these V–P–O catalysts in the production of maleic anhydride [13,14].

As far as the decomposition of 2-propanol is concerned, it has been extensively utilized as a test reaction for the characterization of acid and basic (redox) metal oxide sites [15–20]. The alcohol decomposes through two parallel reactions: dehydration to propene mainly on acid sites, and dehydrogenation to 2-propanone on basic, or concerted acid–base pair sites, or on active sites with redox and basic properties. Some conditions also give rise to the formation of diisopropyl ether by dehydration involving two molecules of 2-propanol, which takes place on acidic sites. However, the role of acidic and basic sites in the formation of propene and 2-propanone still has not been well established. Recently it has been reported as well that the dehydration and dehydrogenation of 2-propanol are also strongly affected by such experimental conditions as reaction temperature, 2-propanol partial pressure and other factors [21,22].

In this respect, our investigation is concerned with the study of some systems based on aluminum–vanadium–phosphorus (AlVPO) prepared by coprecipitation, in a similar way to how amorphous aluminum phosphate ($AlPO_4$) synthesis [23] has been carried out. This is done in order to obtain insight into the effect that the aluminum presence might have on structure, physical and surface properties of V–P–O systems and, consequently, on their catalytic behavior, especially in some oxidation reactions. We found in previous research that the calcination of the AlVPO system over 550 °C promoted an important decrease in catalytic activity not only in the 2-propanol reaction but also in oxidation reactions of benzene, toluene and *o*-xylene, probably related to the structural changes that took place [24]. Thus, the present paper reports on the preparation, characterization and catalytic behavior in the decomposition of 2-propanol on AlVPO systems with several P/V/Al molar ratios, and calcined at 450 and 550 °C, respectively. The materials have been characterized by several physical methods: thermogravimetric analysis (TGA), X-ray diffraction (XRD), diffuse reflectance UV-Vis spectroscopy (UV-Vis), scanning electron microscopy (SEM), ^{27}Al, and ^{31}P MAS NMR, and nitrogen adsorption. Surface acid characterization was also carried out through pyridine chemisorption.

2. Experimental

2.1. Catalysts

The AlVPO systems were prepared from appropriate amounts of NH_4VO_3 reduced with oxalic acid, $AlCl_3{\cdot}6H_2O$, and H_3PO_4 (85 wt.%) by precipitation with aqueous ammonia and stirring at 0 °C until pH 4. After filtration, the solids (AlVPO-I, AlVPO-II and AlVPO-III, where I, II and III indicate the different Al/V molar ratios that decreased from I to III) were calcined in air at 450 and 550 °C for 3 h to obtain six catalysts denominated AlVPO-I-450, AlVPO-I-550, AlVPO-II-450, etc. (as shown in detail in Fig. 1).

As a reference, a VPO system (P/V molar ratio = 1/1.3) was also obtained [24]. H_3PO_4 (85 wt.%) was added to the blue solution of VO^{2+}. The dark green precipitate obtained was washed, dried and calcined in the same way as described above for AlVPO catalysts. Two different catalysts were obtained by calcination at 450 and 550 °C (VPO-450 and VPO-550). All the solids synthesized were screened to <0.149 mm.

2.2. Chemical analysis

The final Al, V and P contents of the catalysts were determined by inductively coupled plasma-atomic emission spectrometry (ICP-AES) analysis on a Perkins Elmer Optima 3000. The samples were completely dissolved in HNO_3, 2 wt.%, diluted to suitable concentrations and measured against standard solutions.

2.3. Textural properties

Surface area and pore size information were obtained from the adsorption–desorption isotherms of nitrogen at its liquid temperature, using a Micromeritics ASAP 2000 apparatus. Prior to measurements, all the samples were degassed to 0.1 Pa. BET surface areas were calculated assuming a cross-sectional area of 0.162 nm^2 for the nitrogen molecule.

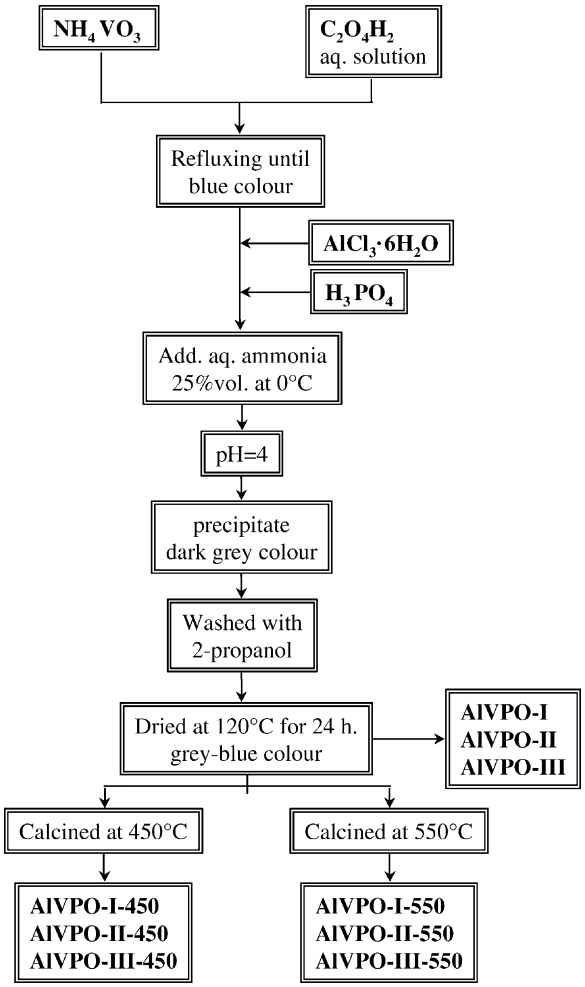

Fig. 1. Schematic drawing of the preparation schedule for AlVPO systems.

2.4. Thermogravimetric analysis

TGA were performed on a Cahn 2000 thermobalance in the presence of static air with a 21 mg sample. The heating rate was 10 °C min^{-1} (temperature range: 30–800 °C). The samples used were the dried precipitates (120 °C, 24 h) prior to calcination.

2.5. XRD measurements

XRD patterns were carried out using Ni-filtered Cu Kα radiation ($\lambda = 1.5418$ Å). Finely ground samples were scanned at a speed of 2° min^{-1} ($2\theta = 10$–$50°$) using a Siemens D-500 difractometer (35 kV, 20 mA).

2.6. NMR spectroscopy measurements

^{27}Al (pulse: 2 μs; recycle delay: 2 s) and ^{31}P (pulse: 2.6 μs; recycle delay: 6 s) MAS NMR spectra were recorded at resonance frequencies of 104.26 and 161.98 MHz, respectively, with a Bruker ACP-400 multinuclear spectrometer (external magnetic field, 9.4 T). All the measurements were carried out at room temperature with a standard Bruker double-bearing MAS (5.5 kHz) probe. About 200 mg of sample material was placed in the rotor with a volume of about 0.35 cm^3. $Al(H_2O)_6{}^{+3}$ and H_3PO_4 solutions were used as external standard references for Al and P chemical shifts, respectively. In order to preserve quantitative analysis, no mathematical procedures of NMR signal treatment, such as multiplication by an exponential function, were used. Also, the chemical shifts given for aluminum were not corrected for second-order quadrupole effects.

2.7. UV-Vis diffuse reflectance spectroscopy

Diffuse reflectance spectra in the UV-Vis region (200–800 nm) were collected with a Variant Cary 1E UV-Vis spectrophotometer equipped with a reflectance attachment using polytetrafluoroethylene as reference.

2.8. Scanning electron microscopy

SEM studies were carried out in a Jeol apparatus, model JSM6300, equipped with an Oxford Instruments detector model link ISIS.

2.9. Surface acid properties

The surface acidity (Bronsted- and Lewis-acid sites) was measured in a dynamic mode by means of the gas-phase adsorption of pyridine (Py) at 100, 200 and 300 °C, using a pulse chromatographic technique [11]. The pulse size was in the range of gas chromatography linearity, corresponding to 0.1–0.5 monolayer. The acidity measurements were repeated several times

and good reproducibility of the results was obtained (ca. 7%).

2.10. 2-Propanol conversion

The 2-propanol conversion (dehydration and dehydrogenation) process was studied by using a microcatalytic pulse reactor inserted between the sample inlet and the column of a HP-5890 II GC. Initially a series of pulses of varying sizes were injected into the catalyst in order to optimize the pulse size within the linear range of the adsorption isotherm. Thus, catalytic measurements were performed under the following conditions: 2-propanol (liquid) volume/pulse size 2 μl; reaction temperature, 170–250 °C (at 40 °C intervals); catalyst weight, 20 mg; flow rate of nitrogen carrier gas, 10 cm^3/min. Before the experiments, the samples were pretreated by in situ heating under nitrogen (10 cm^3/min) for 30 min at 300 °C. The 2-propanol pulses were injected successively till constant values of conversion and yield of products were attained (usually after 3–4 pulses). The final values reported are the mean of values obtained in three or four successive pulses after the stationary state of activity was obtained.

The reaction products: propene, 2-propanone and diisopropyl ether, were analyzed by GC with FID detection. The column was 2 m long (1/8 in., stainless-steel) packed with 5% celanesse-ester on Chromosorb G AW-DMCS 80/100 at 50 °C. A blank test showed the absence of thermal reaction in the absence of the catalyst.

3. Results and discussion

3.1. Chemical composition

The final P, Al and V contents of AlVPO and VPO systems are shown in Table 1. On going from AlVPO-I to AlVPO-III, the vanadium content increased by a factor of 3 (Al content decreased to the same degree). Furthermore, the P/V + Al molar relation for the AlVPO systems, similar to that for the VPO systems, was between 0.7 and 0.8. Only the AlVPO-III systems showed a lower value equal to 0.5–0.6. No changes were observed in either AlVPO or VPO samples subjected to thermal treatment.

3.2. TGA measurements

TG profiles of AlVPO samples were very similar and they were all characterized by two weight losses up to 400 °C. The first one, under 200 °C, can be attributed to the desorption of physically adsorbed water and 2-propanol, while the second one, between 200 and 400 °C, is higher and can be associated to the removal of ammonium chloride. The final weight losses were 38.8, 30.5 and 34.8 for AlVPO-I, II and III, respectively. At temperatures over 400 °C, slight

Table 1
Chemical composition, textural properties and surface acidity versus pyridine, of different systems

Catalyst	Chemical composition (mol%)			Al/V (M)	S_{BET} (m^2/g)	V_p (ml/g)	Py (μmol/g)	
	Al	V	P				100 °C	200 °C
AlVPO-I	41.1	17.2	41.7	2.34	43.2	0.20	–	–
AlVPO-I-450	40.0	17.5	41.5	2.32	17.7	0.05	9.9	5.6
AlVPO-I-550	41.2	17.3	41.5	2.39	2.7	–	–	–
AlVPO-II	29.1	30.8	40.1	0.94	12.0	0.08	–	–
AlVPO-II-450	28.6	30.6	40.8	0.93	4.3	0.01	2.6	–
AlVPO-II-550	27.0	30.9	42.1	0.87	1.0	–	–	–
AlVPO-III	15.3	50.1	33.4	0.31	4.8	0.03	–	–
AlVPO-III-450	16.1	50.0	33.9	0.32	1.9	–	–	–
AlVPO-III-550	15.1	49.2	35.7	0.31	1.4	–	–	–
VPO	–	57.1	42.9	–	2.0	–	–	–
VPO-450	–	56.4	43.6	–	1.8	–	–	–
VPO-550	–	57.5	42.5	–	0.9	–	–	–

weight losses (<2 wt.%) were observed that could be due mainly to the condensation of surface hydroxyls, as occurred in $AlPO_4$–metal oxide systems [7,9,10], and/or to dehydration of the vanadyl hydrogenphosphate hydrates [2]. VPO systems displayed almost the same behavior as previously described [24].

3.3. Textural properties

The nitrogen isotherms obtained for AlVPO and AlVPO-I-450 samples were type IV of the BDDT classification [25], exhibiting H1 hysteresis loops which corresponded to mesoporous solids [26]. The other AlVPO systems, as well as the AlVPO-I, after heating at 450 °C, displayed reversible Type II isotherms that corresponded to non-porous adsorbents. Table 1 compiles the values of BET surface area, S_{BET}, for all solids, and the pore volumes, V_p for those solids with porosity. The S_{BET} values decreased as the amount of vanadium increased. In addition, AlVPO catalysts showed surface areas appreciably higher than VPO catalysts.

3.4. XRD measurements

Fig. 2 shows the XRD patterns of all AlVPO systems. The XRD patterns of the uncalcined AlVPO systems suggest that they were poorly crystallized, since no characteristic peaks can be easily indexed. Reflections relative to β-$VOPO_4$ (JCPDS 27-948) and to $AlPO_4$ crystallized in α-cristobalite form (JCPDS 11-500) were observed after calcination at 450 °C. The crystalline character of both compounds increased with vanadium content in the solids, especially β-$VOPO_4$, and with thermal treatment. Also, the AlVPO-I-450 and AlVPO-II-450 diffractograms exhibited two new lines. There was a small one at $2\theta = 15.5°$ ($d = 5.65$ Å), characteristic of $VOHPO_4{\cdot}0.5H_2O$, and the other one was at $2\theta = 20.5°$ ($d = 4.36$ Å), which is incompatible with the orthorhombic symmetry of α-cristobalite but may be related to the presence of structural defects [7]. Both of them either disappeared or showed appreciably decreased intensities after calcining the solids at 550 °C. As far as the diffractograms of the calcined AlVPO-III systems were concerned, new lines appeared at $2\theta = 15.4°$ ($d = 5.76$ Å), $2\theta = 20.16°$ ($d = 4.4$ Å) and $2\theta = 31.8°$ ($d = 2.88$ Å). These increased in intensity in the sample calcined at 550 °C which can be indexed to V_2O_5 (JCPDS 9-387). This fact can be explained taking account the lower P/Al+V ratio value, in Table 1, presented by these AlVPO-III systems.

With respect to VPO samples, the uncalcined sample showed a small degree of crystallinity with an XRD pattern corresponding to hemihydrate vanadyl hydrogenphosphate $VOHPO_4{\cdot}0.5H_2O$. In addition,

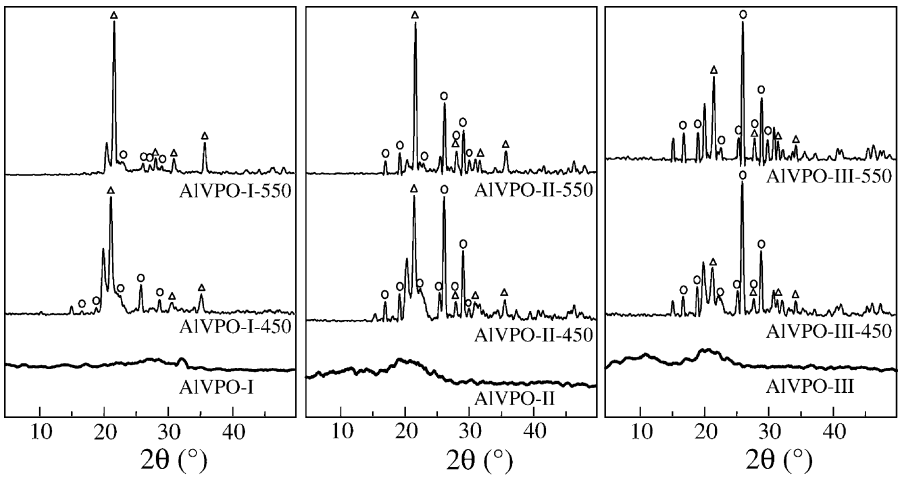

Fig. 2. XRD patterns of uncalcined and calcined AlVPO systems.

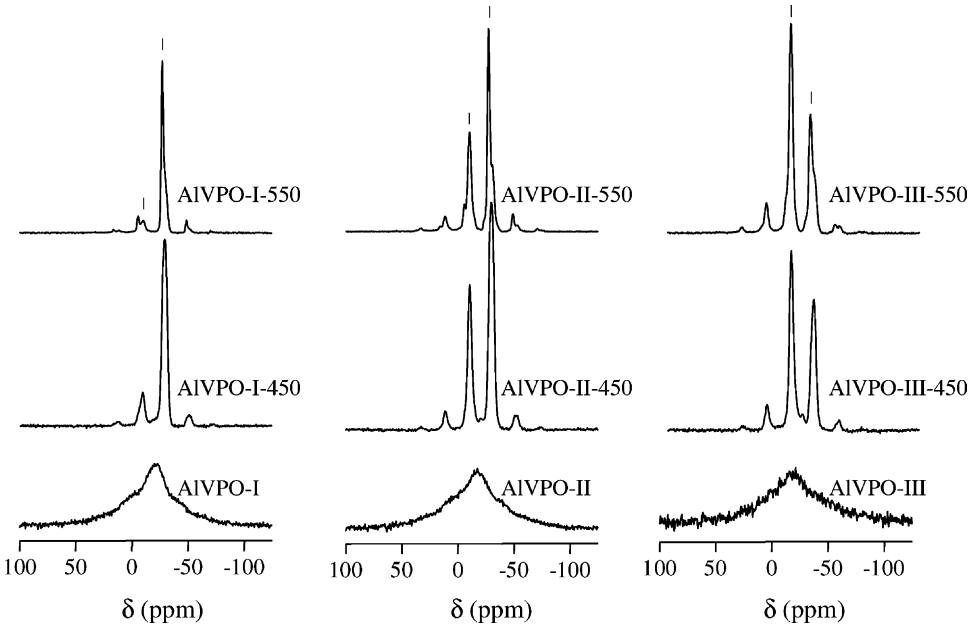

Fig. 3. ^{31}P MAS NMR spectra of uncalcined and calcined AlVPO systems.

VPO samples calcined at 450 and 550 °C turned into fully crystallized β-$VOPO_4$ [24].

3.5. ^{31}P *and* ^{27}Al *MAS NMR spectroscopy*

^{31}P MAS NMR spectra of AlVPO systems are shown in Fig. 3. As can be seen, the spectra of uncalcined AlVPO systems showed a very broad signal. This could be related to the presence of some vanadyl hydrogen phosphate hydrates containing V^{4+}, given the paramagnetic character of this cation [27], and to the mainly amorphous character of the solids in accordance with results from XRD. Similar behavior was reported to uncalcined VPO [24]. However, the spectra of the calcined AlVPO exhibited two major resonances, whose isotropic chemical shift values appeared at around −10 and −29 ppm, and their corresponding spinning sidebands (SSB). The first resonance, which was also displayed in the spectra of calcined VPO systems, can be attributed to β-$VOPO_4$ [27]. The second one corresponded to P atoms in tetrahedral coordination with P–O–Al bonds, i.e. $P(OAl)_4$ environments [7]. The relative intensity of both the resonances was according to the chemical composition of each of the AlVPO systems. Furthermore, both resonances narrowed after calcining the samples at 550 °C, indicating the whole formation and crystallization of the two phases. In addition, those isotropic chemical shift values suffered negligible changes with the composition of the systems, thus implying that there was no change in the electronic environment of the P sites.

^{27}Al MAS spectra of the uncalcined AlVPO, in Fig. 4, also indicated the amorphous character of the systems as well as the presence of mainly tetrahedral Al (peak at around +41 ppm) with some octahedral aluminum (peak at around −7 ppm) atoms. As can also be seen in Fig. 4, the thermal treatment caused the disappearance of the −7 ppm signal as well as the narrowing and slight shifting towards a lower frequency value (from +41 to +39.8 ppm) for the tetrahedral aluminum signal. These facts suggest a total removal of water molecules, changing the aluminum atoms from octahedral to tetrahedral coordination, and the crystallization of $AlPO_4$. Thus, a +39 ppm component is typical of tetrahedral aluminum sharing oxygen atoms with four tetrahedra of phosphorous $[Al(OP)_4]$ [7].

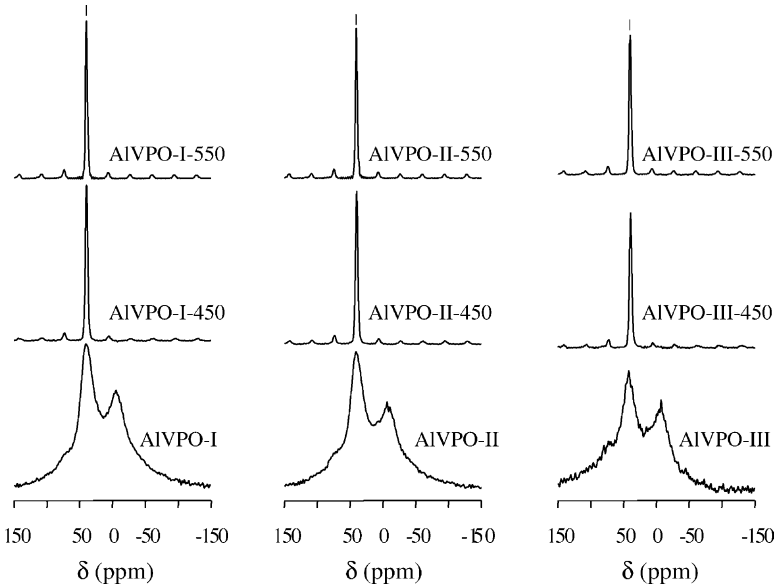

Fig. 4. ^{27}Al MAS NMR spectra of uncalcined and calcined AlVPO systems.

3.6. UV-Vis diffuse reflectance spectroscopy

UV-Vis spectra of uncalcined and calcined AlVPO samples are reported in Fig. 5. In the case of the uncalcined samples, the presence of some absorptions were observed between 550 and 850 nm, which were assigned to d–d transitions of V^{4+} (d^1) [28]. There was also a charge-transfer band at around 240 nm, indicating that V^{4+} ions were present, according to the above results found using other characterization techniques. These bands disappeared after calcination, suggesting that V^{4+} has been mostly oxidized to V^{5+} and, accord-

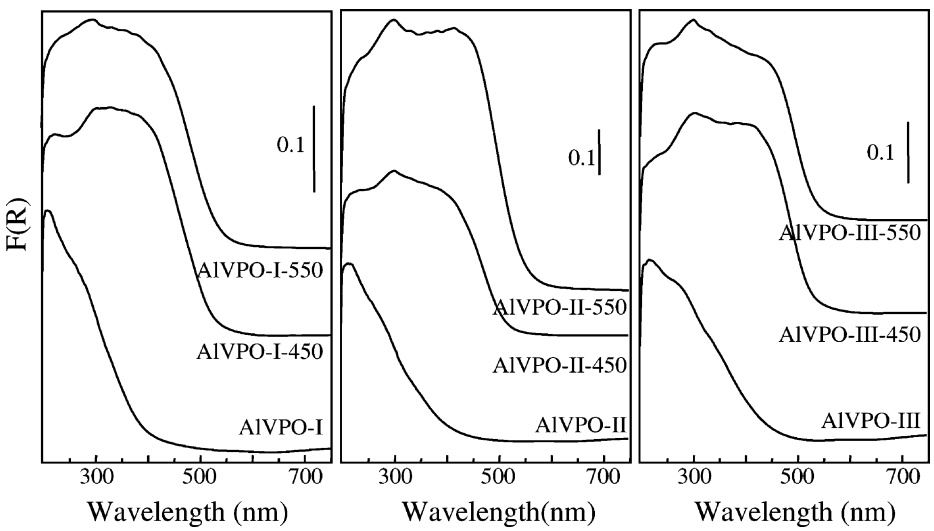

Fig. 5. Diffuse reflectance UV-Vis spectra of uncalcined and calcined AlVPO systems.

ingly, the spectra of calcined AlVPO showed principally charge-transfer bands in the 300–500 nm range, which are characteristic of vanadium compounds with V^{5+} cations in octahedral symmetry [28].

3.7. Scanning electron microscopy

SEM results, Fig. 6, showed a non-homogeneous distribution in morphology, texture and particle size for all uncalcined and calcined AlVPO systems. In addition, the average size of particles decreased slightly and some changes in morphology were also observed, when the vanadium amount and/or the calcined temperature increased. As far as the VPO systems are concerned, the uncalcined one showed a morphology of thin elongated platelets randomly aggregated into non-uniformly sized clumps (Fig. 6(e)). After calcination, the VPO was shown to be quite uniform in size particles formed by randomly oriented angular platelets (Fig. 6(f)). Similar morphologies were previously reported for $VOHPO_4{\cdot}0.5H_2O$ and β-$VOPO_4$, respectively [29].

3.8. Surface acidity measurements

The results obtained in pyridine chemisorption experiments on AlVPO systems calcined at 450 °C are shown in Table 1. The AlVPO system with the high-

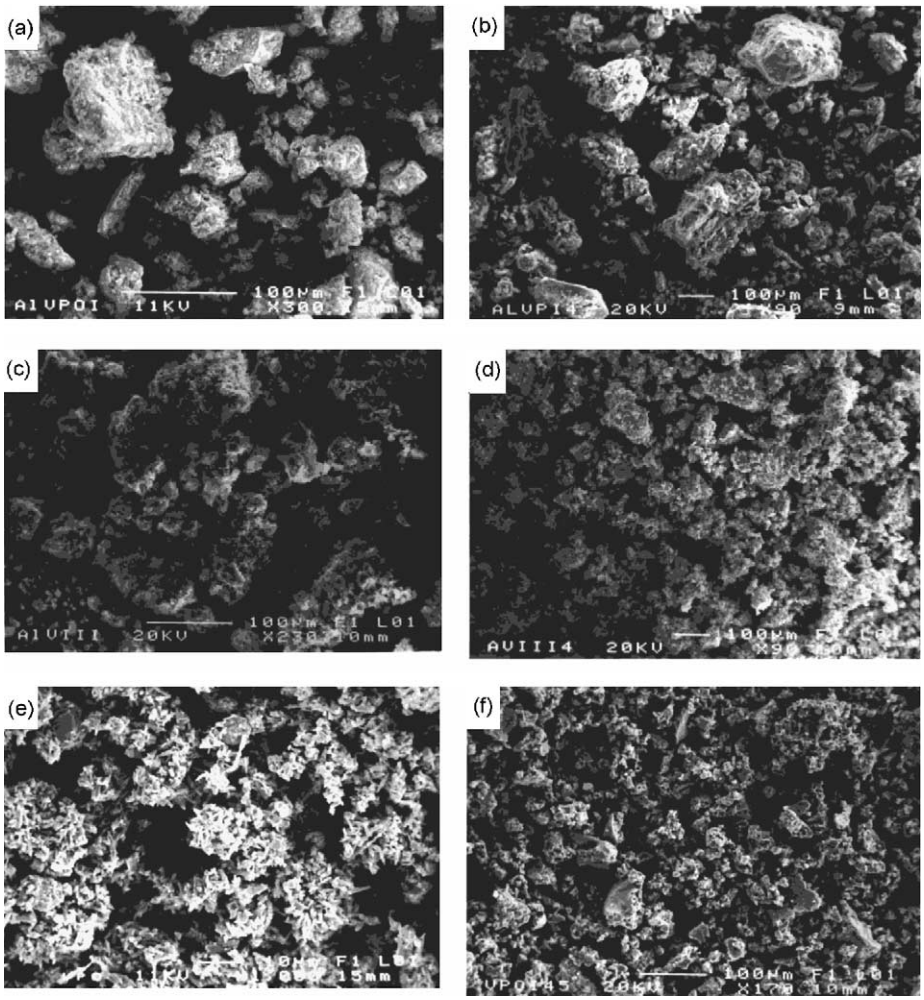

Fig. 6. SEM micrographs: (a) AlVPO-I; (b) AlVPO-I-450; (c) AlVPO-III; (d) AlVPO-III-450; (e) VPO; (f) VPO-450.

est aluminum content not only adsorbed the highest amount of pyridine, but also was able to retain it at the highest temperature, 200 °C (at 300 °C, pyridine was not adsorbed). As a result, both the surface acidity (Bronsted- and Lewis-acid sites) and the strength or energy of those acid sites increased when the aluminum content on AlVPO systems increased. In fact, the AlVPO with the smallest aluminum content (or the highest vanadium content) was not able to retain pyridine at any temperature studied. This same behavior occurred in the VPO systems.

3.9. 2-Propanol conversion

In all the catalysts studied, 2-propanol decomposition produced propene as the major product (selectivity values > 70%) and propanone, as shown in Table 2 where the selectivity values obtained at the

Table 2
Conversion, selectivity, and apparent rate constants for propene ($kK_{C_3H_6}$) and propanone ($kK_{C_3H_6O}$) formation, for 2-propanol decomposition on all catalysts and temperatures studied

Catalyst	T (°C)	Conversion (mol%)	Selectivity (mol%)			$kK_{C_3H_6}$ (μmol/atm m^2 s)	$kK_{C_3H_6O}$ (μmol/atm m^2 s)
			C_3H_6	C_3H_6O	$C_6H_{14}O$		
AlVPO-I-450	*170*	*3.3*	*87.2*[a]	*8.0*	4.8	0.33	0.03
	190	4.8	83.5	5.7	10.8	0.42	0.03
	210	10.4	82.4	4.1	13.5	0.87	0.04
	230	22.0	83.9	2.9	13.3	1.95	0.07
	250	40.4	88.0	2.5	9.5	4.23	0.12
AlVPO-I-550	170	0.2	100	–	–	0.19	–
	190	0.5	79.0	21.0	–	0.32	0.09
	210	1.0	86.4	13.6	–	0.70	0.11
	230	*2.6*	*86.9*	*8.0*	4.7	1.77	0.17
	250	5.7	89.8	5.5	4.7	4.36	0.27
AlVPO-II-450	170	0.7	75.0	25.0	–	0.28	0.09
	190	1.2	74.0	19.0	6.0	0.47	0.12
	210	*2.7*	*76.0*	*14.0*		1.03	0.19
	230	7.0	83.0	8.9	8.1	2.82	0.30
	250	14.8	86.2	6.0	7.8	6.21	0.43
AlVPO-II-550	190	0.1	100	–	–	0.20	–
	210	0.2	100	–	–	0.40	–
	230	0.5	100	–	–	0.90	–
	250	1.4	89.6	10.4	–	2.33	0.27
AlVPO-III-450	190	0.1	100	–	–	0.14	–
	210	0.4	80.2	18.8	–	0.38	0.09
	230	1.4	77.1	13.2	9.7	1.21	0.21
	250	*3.1*	*82.7*	*10.3*	6.9	2.70	0.34
AlVPO-III-550	210	0.3	53.3	46.7	–	0.21	0.19
	230	0.5	68.0	32.0	–	0.45	0.21
	250	1.1	79.1	20.9	–	1.11	0.29
VPO-450	210	0.06	100	–	–	0.11	–
	230	0.2	100	–	–	0.22	–
	250	0.6	79.0	21.0	–	0.44	0.12
VPO-550	210	0.05	100	–	–	0.11	
	230	0.2	60.0	40.0	–	0.33	0.22
	250	0.5	73.0	27.0	–	0.81	0.30

[a] Selectivity values at isoconversion are marked in italics.

170–250 °C temperature range are collected. Diisopropyl ether was also sometimes observed, although the selectivity values attained were rarely higher than 10%. Furthermore, the total conversion of 2-propanol along with the propene selectivity values increased, while the propanone selectivity values decreased with the increasing reaction temperature.

On the other hand, for all the catalysts studied both the dehydration to propene and the dehydrogenation to propanone data, were found to fulfill the Basset–Habgood rate equation [30] for first-order reactions, where the partial reactant pressure is low and the adsorption rate is faster than the rate of surface reaction (the latter being the rate determining step). Thus, only the data for under 20 mol% of 2-propanol conversion, where the equilibrium reaction can be ignored, were used for the calculation. The Basset–Habgood was in the form

$$\ln\left[\frac{1}{1-X}\right] = kKRT\left(\frac{W}{F}\right)$$

where X is the conversion of 2-propanol to propene or to propanone, kK the apparent rate constant of both dehydration and dehydrogenation processes, W the catalyst weight, and F the flow rate of carrier gas.

The kK values, in μmol/atm m^2 s, for propene and propanone formation at each reaction temperature studied for all calcined AlVPO and VPO, are also collected in Table 2. Even when we added the effect of the surface area, those results indicated that in both reactions the AlVPO systems were more active than VPO ones and the activity of the systems increased with the aluminum content and decreased when the calcination temperature increased from 450 to 550 °C. Taking into account the general conclusion that acidic sites on catalyst surfaces catalyze the dehydration of 2-propanol [15,16,18], those sites seem to predominate in our catalytic systems. Furthermore, the presence of aluminum in the precipitation medium of the VPO system would not only generate a higher number of acidic sites but also stronger ones, according to the results obtained in pyridine chemisorption (Table 1). However, the dehydrogenation ability of systems seems to be more related to the amounts of vanadium in the solids. Thus, in general, the values of propanone selectivity increased with the vanadium content in AlVPO systems, the values obtained for the AlVPO-III systems being similar to those obtained for VPO systems, at the reaction temperature where they showed activity (Table 2). In addition, the selectivity values at isoconversion (about 3 mol%; Table 2) again indicated that dehydrogenation took place to a greater extent in the AlVPO systems with the highest vanadium content, since the selectivity depended on temperature. However, considering the basic/redox sites to be necessary for propanone formation [16,17], the presence of $AlPO_4$ could modify their density and/or strength on VPO. This would explain the activity AlVPO systems showed with respect to propanone formation at lower temperature values than VPO ones. It would explain as well the reducibility of AlVPO which took place at lower temperatures, and better catalytic performance than VPO systems, according to TPR experiments and oxidation reactions of hydrocarbons [31], respectively.

On the other hand, Table 3 collects the activation parameters (E_a and $\ln A$) for propene and propanone formation, obtained from the Arrhenius equation by plotting $\ln kK$ values, in Table 2, versus T^{-1} as well as the values of those parameters obtained on AlVPO (P/V/Al = 1 and calcined at 450–750 °C temperature range) systems previously studied [24]. Thus, all catalysts obtained higher activation energy values for propene formation than for propanone formation. These results are in agreement with those reported by Cunningham et al. [32] and Grzybowska-Swierkosz et al. [33] for pure V_2O_5 and V_2O_5/TiO_2 catalysts, respectively. Furthermore, our values range around those found by Cunningham et al. ($E_{a\,C_3H_6}$ = 20 kcal/mol and $E_{a\,C_3H_6O}$ = 14 kcal/mol) and by Grzybowska-Swierkosz et al. ($E_{a\,C_3H_6}$ = 16 kcal/mol and $E_{a\,C_3H_6O}$ = 6 kcal/mol).

The markedly different values of activation energies obtained for both reactions suggest that the dehydration may proceed via a different mechanism than that found in dehydrogenation. This observation is also supported on the basis of different values of the isokinetic parameters in both reactions. These isokinetic parameters were obtained from the relationship found between $\ln A$ and E_a (as shown in Fig. 7), according to the most habitual expression of the "compensation effect" or "isokinetic relationship" [34–36]:

$$\ln A = \ln\alpha + \frac{E_a}{\theta R}$$

where θ is the isokinetic temperature at which identical values of reaction rate constant, α, are obtained. In

Table 3
Activation parameters E_a and $\ln A$ obtained from apparent rate constants in Table 2 with the AlVPO and VPO catalysts, and from apparent rate constants obtained with AlVPO[a] (P/V/Al = 1/0.5/0.5) previously [24]

Catalyst	$E_{a\,C_3H_6}$ (kcal/mol)	$\ln A$ (mol/atm g s)	$E_{a\,C_3H_6O}$ (kcal/mol)	$\ln A$ (mol/atm g s)
AlVPO-I-450	15.0 ± 2.0	4.9 ± 0.6	11.6 ± 0.9	−1.9 ± 0.2
AlVPO-I-550	18.0 ± 1.0	6.1 ± 0.5	9.2 ± 0.9	−5.3 ± 0.6
AlVPO-II-450	18.0 ± 1.0	7.0 ± 0.6	9.3 ± 0.8	−4.2 ± 0.4
AlVPO-II-550	19.0 ± 1.0	5.7 ± 0.4	–	–
AlVPO-III-450	23.0 ± 1.0	10.2 ± 0.6	17.0 ± 2.0	1.8 ± 0.2
AlVPO-III-550	21.7 ± 0.8	7.6 ± 0.3	6.0 ± 1.0	−9.0 ± 2.0
AlVPO-450[a]	26.0 ± 4.0	15.2 ± 2.0	8.4 ± 07	−5.6 ± 04
AlVPO-550[a]	18.0 ± 1.0	5.7 ± 0.5	12.6 ± 0.5	−2.3 ± 0.1
AlVPO-650[a]	20.0 ± 2.0	5.5 ± 0.6	–	–
AlVPO-750[a]	26.0 ± 4.0	11.0 ± 2.0	–	–
VPO-450	17.3 ± 0.4	2.68 ± 0.06	–	–
VPO-550	24.0 ± 1.0	9.4 ± 0.5	–	–

fact, if a compensation effect holds for a reaction series, exhibiting similar isokinetic parameters, a single common interaction mechanism, through a common transition state, can be expected [34–36]. Thus, with the catalysts here studied the propene and propanone formation from 2-propanol decomposition must involve different active sites and/or different intermediates.

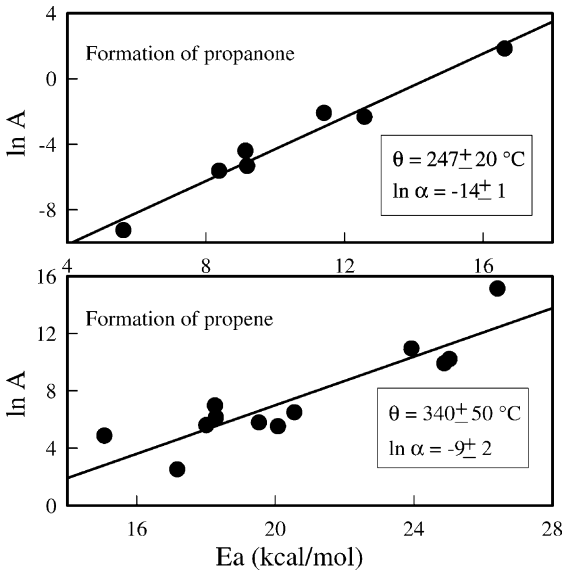

Fig. 7. Compensation effects in the conversion of 2-propanol between $\ln A$ and E_a for different catalysts in Table 3. In both the cases data are fitted with significance levels higher than 99.9%.

4. Conclusions

In summary, significant changes took place in vanadyl phosphate (VPO) surface properties due to the presence of aluminum in its precipitation medium. Thus, the formation of AlVPO systems with some porosity, which increased along with surface areas when the aluminum content increased, was observed through textural analysis. Furthermore, the vanadyl phosphate crystallization process was delayed, showing the amorphous character in uncalcined AlVPO systems independently of Al/V ratio value. This was contrary to uncalcined VPO, which showed some degree of crystallinity. After calcination at 450 °C, the formation of β-$VOPO_4$ and $AlPO_4$ (α-cristobalite) took place, whose crystalline character increased, especially in the case of β-$VOPO_4$, with the vanadium content in the AlVPO systems and with the thermal treatment. In addition, the presence of aluminum produced catalysts that exhibited improved catalytic activity for 2-propanol decomposition. Thus, AlVPO systems were more active than VPO ones, and the activity of AlVPO systems increased with the aluminum content and decreased when the calcination temperature increased from 450 to 550 °C. This occurred in both the dehydration process to propene, which was the more important process, and dehydrogenation to propanone. However, propanone selectivity decreased slightly as the aluminum content increased. These results can be interpreted in terms of the differences in the number and strength of acid

sites (considered to be responsible for dehydration to propene) observed in pyridine chemisorption experiments, and in the modification that could result from the presence of aluminum content in the density and/or strength of VPO basic/redox sites (responsible for dehydrogenation). Furthermore, on all AlVPO and VPO catalysts studied, we propose that dehydration and dehydrogenation of 2-propanol might proceed not only through different active sites but also via different mechanisms, according to the differences obtained in the activation parameters for the two processes.

Acknowledgements

The authors gratefully acknowledge the subsidies granted by the Ministerio de Ciencia y Tecnología, project BQU2001-2605, co-financed by FEDER funds, and by the Consejería de Educación y Ciencia (Junta de Andalucia), Spain. The valuable help of Prof. M. Sullivan in the grammatical revision of the manuscript is also acknowledged.

References

[1] G. Centi (Ed.), Catalysis Today, vol. 16, 1993.
[2] E. Bordes, Catal. Today 1 (1987) 499.
[3] F. Trifirò, Catal. Today 41 (1998) 21.
[4] G.J. Hutchings, Appl. Catal. 72 (1991) 1.
[5] V.V. Guliants, J.B. Benziger, S. Sundaresan, I.E. Wachs, J.-M. Jehng, J.E. Roberts, Catal. Today 28 (1996) 275.
[6] J.M. Campelo, A. García, D. Luna, J.M. Marinas, M.S. Moreno, J. Colloid Interf. Sci. 118 (1987) 98.
[7] F.M. Bautista, J.M. Campelo, A. Garcia, D. Luna, J.M. Marinas, A.A. Romero, Appl. Catal. A 96 (1993) 175.
[8] T. Lindblad, B. Rebenstorf, Z.-G. Yan, S.L.T. Andersson, Appl. Catal. A 112 (1994) 187.
[9] F.M. Bautista, J.M. Campelo, A. Garcia, D. Luna, J.M. Marinas, A.A. Romero, G. Colon, J.A. Navio, M. Macias, J. Catal. 179 (1998) 483.
[10] F.M. Bautista, J.M. Campelo, A. Garcia, D. Luna, J.M. Marinas, M.C. Moreno, A.A. Romero, J.A. Navio, M. Macias, J. Catal. 173 (1998) 333.
[11] F.M. Bautista, J.M. Campelo, A. Garcia, D. Luna, J.M. Marinas, M.R. Urbano, J. Mater. Chem. 4 (1994) 311.
[12] T. Mishra, K.M. Parida, S.B. Rao, Appl. Catal. A 166 (1998) 115.
[13] P.S. Kuo, B.L. Yang, J. Catal. 117 (1989) 301.
[14] S. Holmes, L. Sartoni, A. Burrows, V. Martin, G.J. Hutchings, Ch. Kiely, J.-C. Volta, Stud. Surf. Sci. Catal. 130 (2000) 1709.
[15] M. Ai, J. Catal. 60 (1979) 306.
[16] B. Grzybowska-Swierkosz, Mater. Chem. Phys. 17 (1987) 121.
[17] C. Lahousse, J. Bachelier, J.C. Lavalley, H. Lauron-Pernot, A.M. Le Govic, J. Mol. Catal. 87 (1994) 329.
[18] F.M. Bautista, J.M. Campelo, A. García, D. Luna, J.M. Marinas, A.A. Romero, M.R. Urbano, Catal. Lett. 35 (1995) 143.
[19] M.A. Aramendía, V. Borau, C. Jiménez, J.M. Marinas, A. Porras, F.J. Urbano, J. Catal. 161 (1996) 829.
[20] V.K. Díez, C.R. Apesteguía, J.I. Di Cosimo, Catal. Today 63 (2000) 53.
[21] J.A. Wang, X. Bokhimi, O. Novaro, T. López, F. Tzompantzi, R. Gómez, J. Navarrete, M.E. Llanos, E. López-Salinas, J. Mol. Catal. A 137 (1999) 239.
[22] J.E. Rekoske, M.A. Barteau, J. Catal. 165 (1997) 57.
[23] J.M. Campelo, A. García, D. Luna, J.M. Marinas, J. Catal. 111 (1988) 106.
[24] F.M. Bautista, J.M. Campelo, A. García, D. Luna, J.M. Marinas, A.A. Romero, M.T. Siles, Stud. Surf. Sci. Catal. 130 (2000) 803.
[25] S. Brunauer, L.S. Deming, W.S. Deming, E. Teller, J. Am. Chem. Soc. 62 (1940) 1723.
[26] K.S.W. Sing, D.H. Everett, R.A.W. Haul, L. Moscou, R.A. Pierotti, J. Rouquerol, T. Siemieniewska, Pure Appl. Chem. 57 (1985) 603.
[27] N.H. Batis, H. Batis, A. Ghorbel, J.C. Vedrine, J.C. Volta, J. Catal. 128 (1991) 248.
[28] G. Lischke, W. Hanke, H.-G. Jerschkewitz, G. Öhlmann, J. Catal. 91 (1985) 54.
[29] C.J. Kiely, A. Burrows, S. Sajip, G.J. Hutchings, M.T. Sananes, A. Tuel, J.C. Volta, J. Catal. 162 (1996) 31.
[30] D. Basset, H.W. Habgood, J. Phys. Chem. 64 (1960) 769.
[31] F.M. Bautista, J.M. Campelo, A. García, D. Luna, J.M. Marinas, A.A. Romero, M.T. Siles, in preparation.
[32] J. Cunningham, B.K. Hodnett, M. Ilyas, J. Tobin, E.L. Leahy, J.L.G. Fierro, Faraday Discuss. Chem. Soc. 72 (1981) 283.
[33] B. Grzybowska-Swierkosz, G. Coudurier, J.C. Vedrine, I. Gressel, Catal. Today 20 (1994) 165.
[34] A. Corma, F. Llopis, J.B. Monton, S. Weller, J. Catal. 142 (1993) 97.
[35] E. Grinwald, C. Steel, J. Am. Chem. Soc. 117 (1995) 5687.
[36] J.J. Roney, Catal. Lett. 50 (1998) 15.